

Effect of Austenite Stability on Pack Aluminizing of Austenitic Stainless Steels

CHRISTOPHER LOPEZ,¹ ARMEN KVRAN,¹ SHAHAN KASNAKJIAN,²
ARMANDO CORONADO,¹ SUTINE SUJITTOSAKUL,¹
OBED VILLALPANDO,² and VILUPANUR A. RAVI^{1,3}

1.—Department of Chemical & Materials Engineering, California State Polytechnic University, Pomona, CA 91768, USA. 2.—Department of Mechanical Engineering, California State Polytechnic University, Pomona, CA 91768, USA. 3.—e-mail: vravi@csupomona.edu

Aluminide coatings were applied to the surfaces of several austenitic stainless steels—UNS S30300, S30400, S30900, S31000, and S31600 (Type 303, 304, 309, 310, and 316)—by the halide activated pack cementation process. The coating compositions, microstructures, and hardness were determined for the different steels coated at 850°C for 25 h. The stability of the austenite phase for each type of steel was calculated by determining the ratio of the nickel to the chromium equivalents based on their nominal compositions. The thickness of the inner diffusion zone in the coating was shown to be inversely related to the austenite stability of the steels. Microhardness measurements were obtained across the coating thickness and into the substrate. The hardness values followed the same trends as the aluminum composition profile into the substrate.

INTRODUCTION

Current industrial processes require stainless steels to endure higher temperatures in order to increase efficiency. In high-temperature applications (>550°C), it is important to consider the mechanical strength of the materials of construction as well as their capacity to resist environmental attack. The petroleum,¹ nuclear,² and power generation³ industries are some of those affected by these enhanced requirements. Selecting materials for these punishing environments can take two broad directions: (I) designing new alloys or (II) depositing a coating on the substrate.⁴ Forming new alloys can be expensive, and a lack of long-term field data dissuades further investment into the alloy. A lower cost alternative would be to apply a protective coating to the currently used material or component. Some issues to be considered include joining and repair.

Diffusional coatings offer superior adhesion and conformance to the substrate. One method of applying a diffusional coating is halide-activated pack cementation (HAPC). HAPC is a chemical vapor deposition process in which the coating element undergoes a disproportionation reaction and diffuses into the substrate.^{5,6} This process minimizes

line-of-sight issues for many component geometries.⁵ Recent studies in aluminized coatings on stainless steels using HAPC have focused on tailoring process parameters to achieve coatings of a desired thickness and composition, e.g., the kinetics of aluminide coating growth on austenitic S30400 steel,^{7–9} the effect of the halide activator on alloy steels,¹⁰ and the stability of the coatings formed.¹¹

In other earlier studies,¹² aluminide coatings deposited via pack cementation on two austenitic stainless steel substrates (S31600 and S31000) were analyzed in the context of austenite stability (nominally the ratio of nickel to chromium equivalents), and a relationship between coating thickness and austenite stability was determined. In a recent study,⁹ UNS S30300, S30400, S30900, S31000, and S31600 alloys were chosen to expand the investigation of the effect of austenite stability on HAPC aluminide coatings (Table I). In this article, the relationship between the austenite stability of various alloys and the coating thickness, morphology, and properties is reported.

MATERIALS AND METHODS

Test coupons (~12.7 mm in diameter × 2.9 mm thick) were cut from as-received stainless steel rods

and the flat faces were ground to a 600-grit finish. They were weighed, measured, cleaned with soap and water, and finally ultrasonically degreased in acetone. An inert filler, master alloy, and halide activator were blended thoroughly to make up the pack. The coupon was then buried in the powder mixture and placed in a ceramic crucible. The crucible was sealed with ceramic cement and placed in a tube furnace. The furnace was heated to 850°C and held at temperature for periods varying from 1–25 h in a flowing inert gas environment. After the coating process was completed, the coupons were extracted from the pack and analyzed using x-ray diffraction (surface analysis). The coupons were also cross-sectioned, mounted, and characterized using optical microscopy, scanning electron microscopy (SEM), and Vickers microhardness. The austenite stability was determined

based on Hammar and Svensson's chromium and nickel equivalents.^{13,14}

Coating thickness measurements were made using optical micrographs of the cross-sections. Twenty images were obtained from different areas across each coupon. In each of these images, thickness measurements were made at five evenly spaced locations for each micrograph. Mean thickness values were computed from a collection of 100 measurements per coupon. Standard deviations and coefficients of variation of the thicknesses were also calculated to provide insights into the variability of the coatings.

RESULTS AND DISCUSSION

Figure 1 shows optical micrographs of the cross-sections of five different austenitic stainless steels (in the order of increasing austenite stability):

Table I. Nominal Alloy Compositions (wt.%) for the Austenitic Stainless Steels Used in this Study¹⁶

Alloy	Cr	Mo	Si Maximum	Ni	Mn	C Maximum	S	P Maximum
S30400	19	0.6	1	10	2	0.08	0.030 maximum	0.045
S30300	18	0.6	1	9	2	0.15	0.15 minimum	0.20
S31600	17	2.5	1	12	2	0.08	0.030 maximum	0.045
S30900	23	0.6	1	13.5	2	0.2	0.030 maximum	0.045
S31000	25	0.6	1.5	20.5	2	0.25	0.030 maximum	0.045

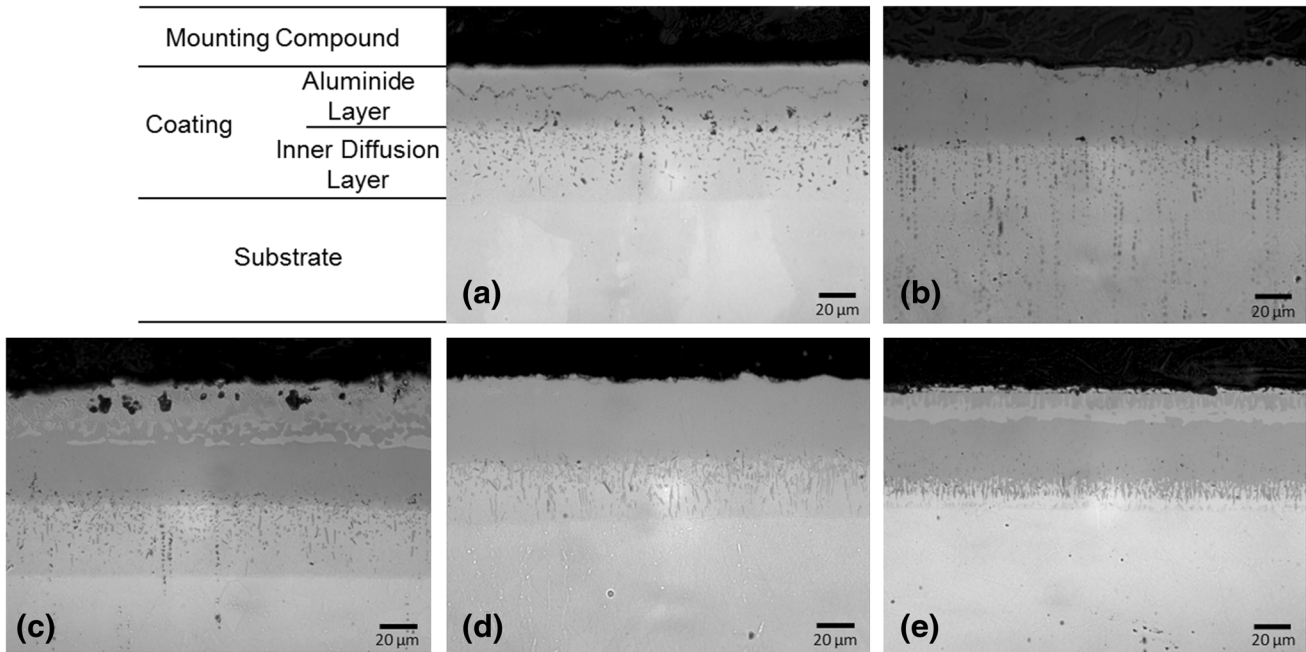


Fig. 1. Optical micrographs of the cross sections of aluminized austenitic stainless steels coated at 850°C for 25 h, in order of increasing austenite stability, UNS (a) S30400, (b) S30300, (c) S31600, (d) S30900, and (e) S31000 steels. (Note the vertical striations are MnS stringers, particularly pronounced in the S30300 coupon.) The location of the mounting compound, the coating and the substrate are pointed out in the schematic attached to (a).

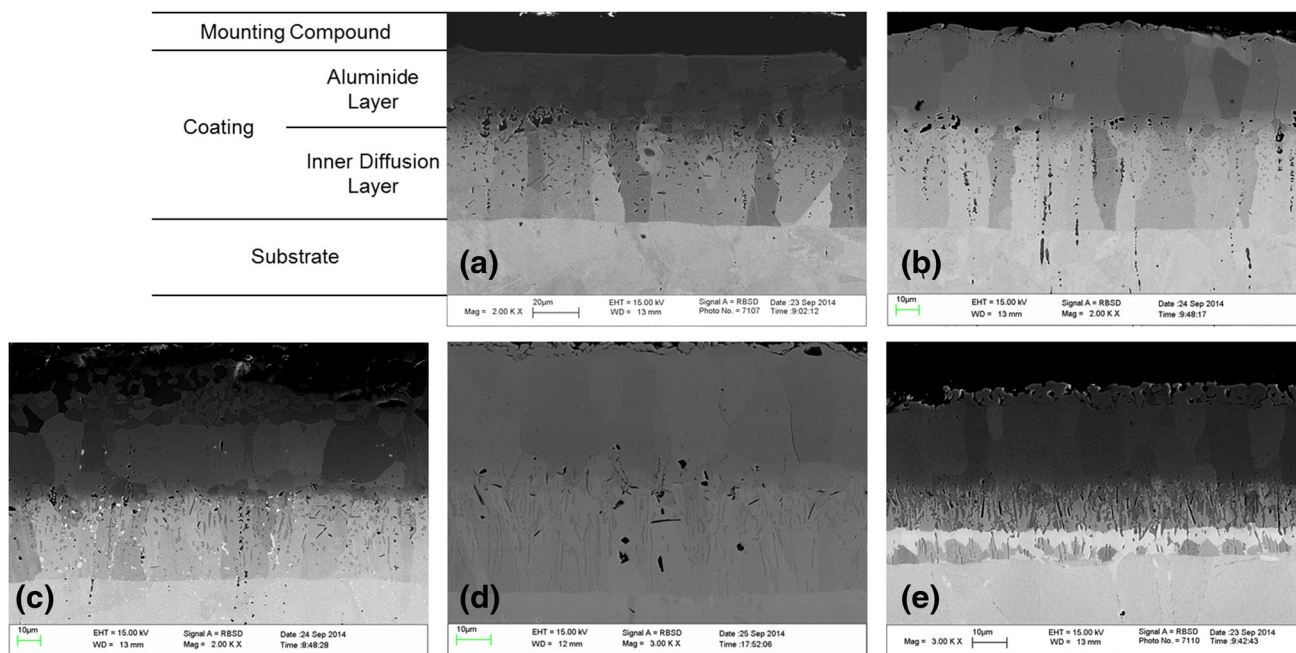


Fig. 2. Backscattered electron images (BEIs) of the cross sections of aluminized austenitic stainless steels coated at 850°C for 25 h, in order of increasing austenite stability, UNS (a) S30400, (b) S30300, (c) S31600, (d) S30900, and (e) S31000 steels. (Note the vertical striations are MnS stringers, particularly pronounced in the S30300 coupon.) The location of the mounting compound, the coating, and the substrate are pointed out in the schematic attached to (a).

S30400 (Fig. 1a), S30300 (Fig. 1b), S31600 (Fig. 1c), S30900 (Fig. 1d), and S31000 (Fig. 1e) coated at 850°C for 25 h. The coatings on S30400, S30300, and S30900 have two distinct layers, an outer aluminide layer and an inner diffusion zone, whereas the S31600 and S31000 have nominally three layers. The outer-most zone is most likely a cemented layer¹² with the intermediate aluminide layer and the inner diffusion zone located beneath it. Within the inner diffusion zone, long needlelike features were more prominent in S31000, less so in S31600 and S30900, and more rounded in S30400 and S30300, correlating with the respective austenite stability for each of the steels.¹² Stringers of manganese sulfide are particularly notable in the S30300 steels. These steels are formulated with high sulfur and manganese contents to defend against hot shortness and to improve machinability.¹⁵

Figure 2 shows backscattered electron images of the cross-sections of aluminized stainless steels coated at 850°C for 25 h. Large grains characterize the predominantly single-phase outer aluminide layers, while the inner layers contain two or more phases in all of the steel coupons. Manganese sulfide stringers are visible in the S30300 coupon. The presence of some pores at the interface between the outer coating layer and the inner diffusion zone points to some amount of outward diffusion of nickel even in a high-activity aluminum pack where inward diffusion of aluminum dominates.

Further supportive evidence for outward nickel diffusion is shown in the elemental maps of the S31000 coupon in Fig. 3, where an absence of nickel was detected in the chromium-rich lower portion of the inner diffusion zone. Continued growth of nickel aluminide is facilitated by the consumption of nickel at the interface between the coating and the original substrate surface. Once a significant amount of nickel is removed from the substrate surface, the austenite phase loses stability and is subsequently transformed into the ferrite matrix. The mobility of aluminum in ferrite is significantly higher than in austenite, leading to thicker aluminide coatings in stainless steels with lower austenite stability.¹² The evolution of the outer aluminide coating from a nickel-containing iron aluminide to predominantly iron aluminides is illustrated by the XRD patterns of the surface of as-coated S31000 steel after aluminizing (Fig. 4). The aluminized surface initially consists of Al_5FeNi and AlFe for short coating times (1 h), transforms to predominantly Al_5FeNi for intermediate coating times (16 h), and at even longer coating times changes to AlFe_3 and Al_3Fe_2 . The thermodynamic stability of the Al_3Fe_2 phase and the beneficial effects of this phase in regards to oxidation resistance in low chromium steels have been reported in the literature.¹¹

Figure 5a shows a secondary electron image of the cross-section of an aluminized S31000 coupon.

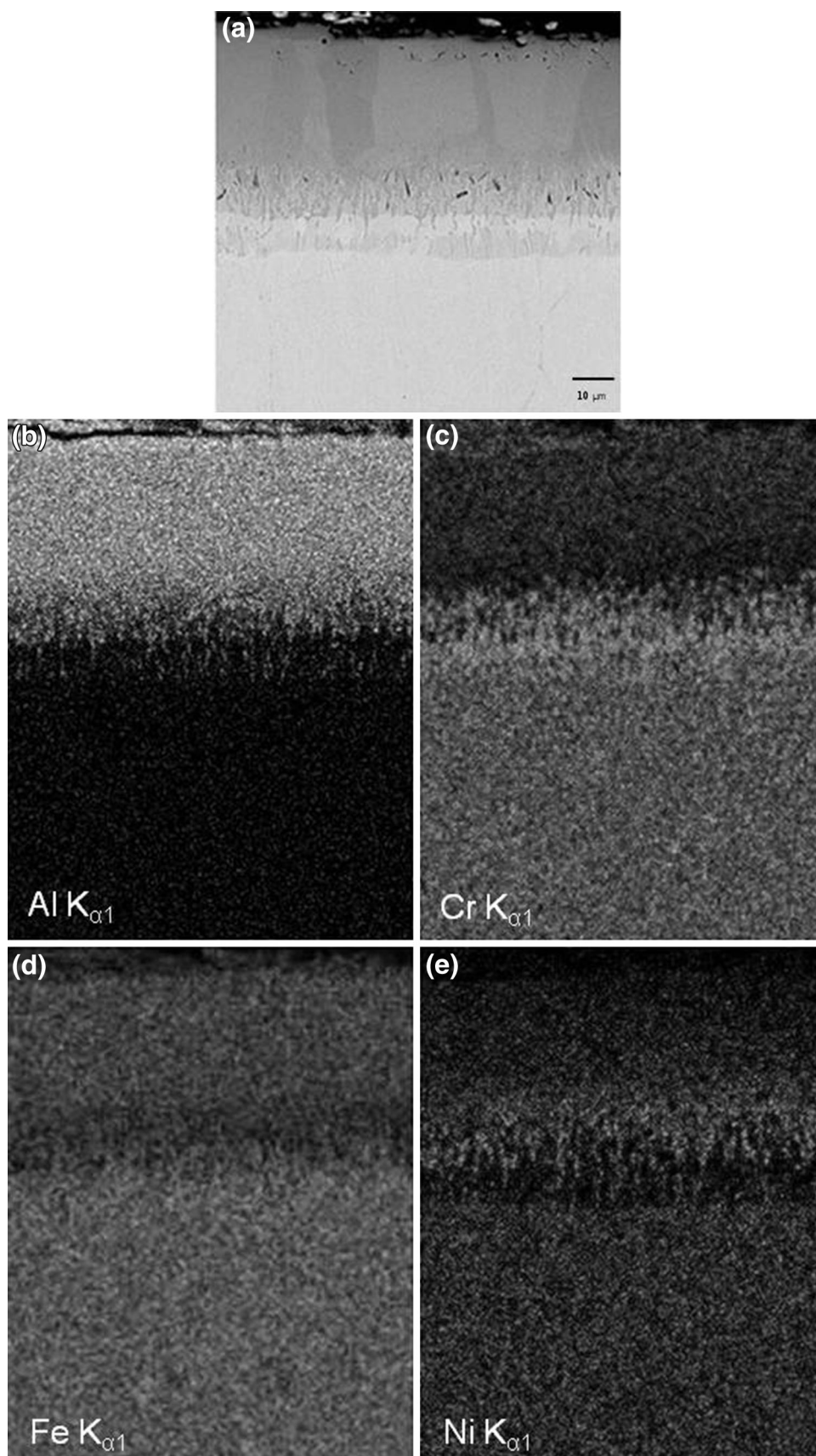


Fig. 3. (a) Backscattered electron image of the cross section of UNS S31000 aluminized at 850°C for 25 h with elemental maps, (b) aluminum, (c) chromium, (d) iron, and (e) nickel.

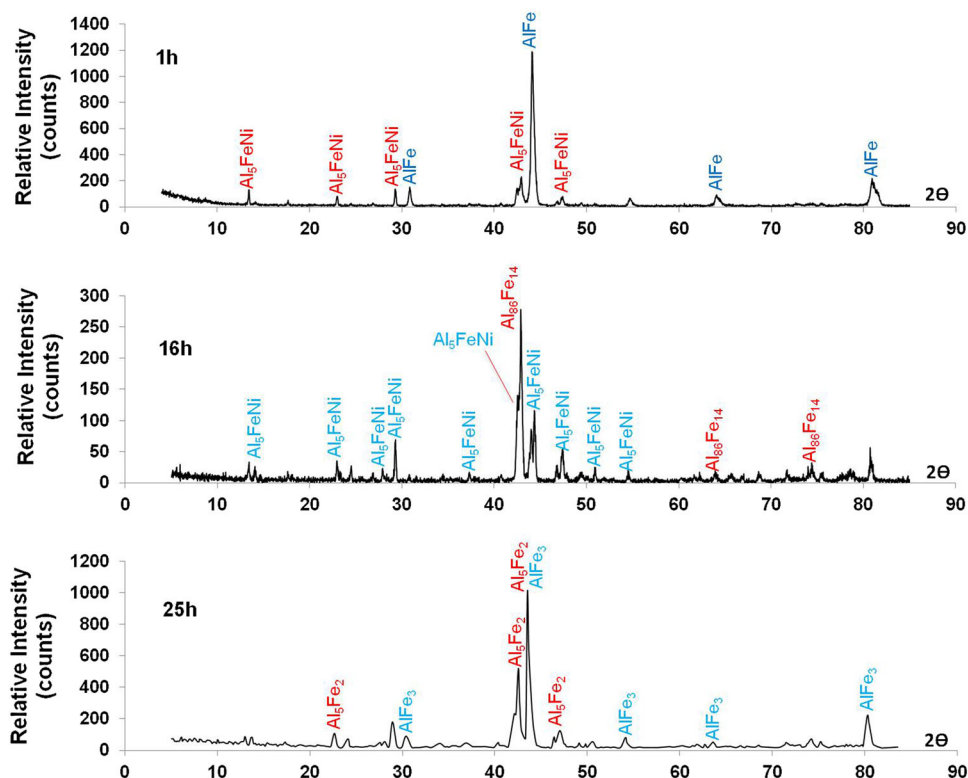


Fig. 4. X-ray diffraction patterns of the aluminized surfaces of UNS S31000 coated at 850°C for 1 h, 16 h, and 25 h.

The concentration profiles of the constituent elements and a plot of Vickers microhardness profile (measured from the outer edge of the coating at an applied load of 10 gf) are shown in Fig. 5b and c, respectively. For the coupons tested, the outer layer of the coating was the hardest layer formed. The hardness values decrease from the outside of the coating deeper into the substrate.

Table I shows the elemental compositions of the stainless steels used in this study.¹⁶ Table II shows the Ni and Cr equivalents, as well as the austenite stability for the above alloys.

As shown in Fig. 6, the stability of the austenite phase is inversely correlated with the thickness of the inner diffusion zone of the aluminide coating; i.e., as the stability of the austenite increased, the resultant coating thickness decreased, for a given set of coating conditions. For low austenite stability alloys, the outward nickel diffusion and subsequent interaction with the inwardly diffusing aluminum results in the transformation of the nickel-depleted austenitic to the ferritic phase. Aluminum diffusion in the ferritic phase is significantly higher than in the austenite phase. For the alloys with high austenite stability, the inward diffusion of aluminum is limited due to

the plentiful supply of austenite stabilizers (Ni in particular). The higher nickel content in these alloys ensures that even after forming aluminides, there is sufficient nickel to continue stabilizing the austenite phase. Without the formation of ferrite, the diffusion of aluminum becomes quite limited, thereby resulting in a thinner diffusion zone.

SUMMARY AND CONCLUSION

Several austenitic stainless steels—UNS S30400, S30300, S31600, S30900, and S31000—were aluminized using the HAPC process. Coatings produced at 850°C for 25 h were characterized using optical microscopy, x-ray diffraction, Vickers microhardness and SEM/EDS. These coatings consisted of an outer aluminide layer, an intermediate zone that is nickel rich, and a nickel-depleted and chromium-rich inner zone. Austenite stabilities were computed for the different steels, with S31000 having the highest austenite stability and S30400 the least. As the stability of the austenite increased, the thickness of the inner diffusion zone in the coating decreased in an exponential fashion. This was attributed to the higher resistance to aluminum

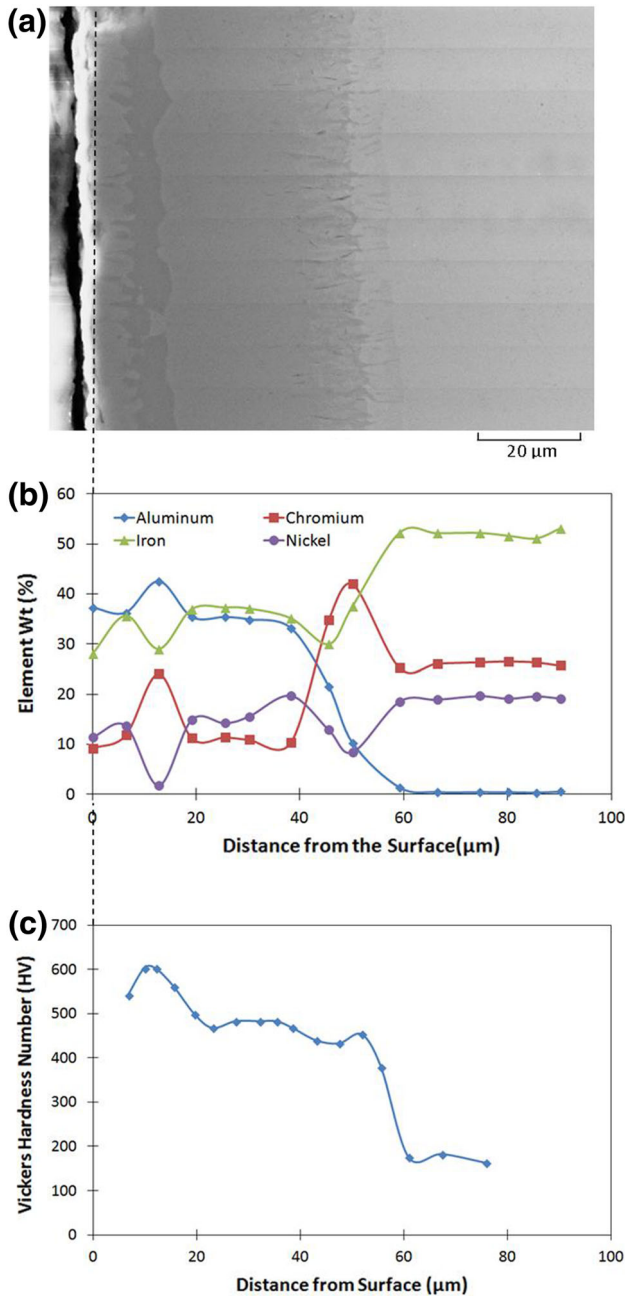


Fig. 5. (a) Secondary electron image, (b) concentration profiles of the major alloying elements, and (c) Vickers microhardness (applied load = 10 gf) profiles for UNS S31000 coated at 850°C for 25 h, showing the correlation of microstructure, hardness and elemental concentration for this aluminized stainless steel.

diffusion in high-austenite-stability alloys and the easier aluminum ingress into low-austenite-stability alloys. Microhardness values tracked the aluminum concentration.

Table II. Austenite stabilities calculated from Ni and Cr equivalents

Alloy	Cr equivalent	Ni equivalent	Austenite stability
S30400	21.32	12.38	0.58
S30300	20.32	12.92	0.64
S31600	21.93	14.38	0.66
S30900	25.32	18.52	0.73
S31000	28.07	26.62	0.95

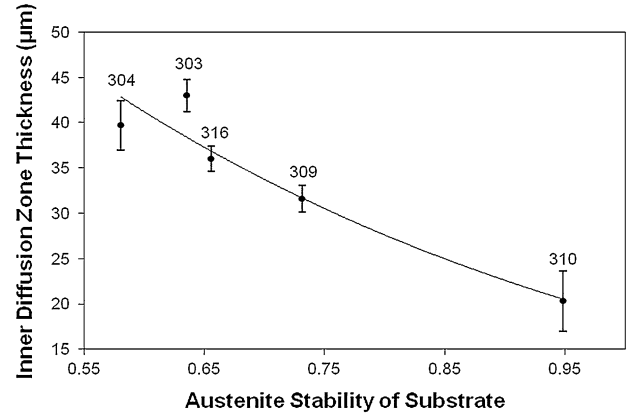


Fig. 6. The inner diffusion zone thickness versus austenite stability for different austenitic stainless steels coated at 850°C for 25 h, showing the inverse relationship between the thickness of this zone and austenite stability. Data points represent average thickness values ($N = 100$) with the error bars denoting ± 1 standard deviation.

ACKNOWLEDGEMENTS

The authors would like to acknowledge Fatin Hanani Ismail, Zorineh Megerdichian, Sarah Phipps, Brian Stoops, and Mr. Ulus Ekerman (all from Cal Poly Pomona) for experimental support. FE-SEM and EDS analyses were done at the Caltech GPS analytical facility, which is supported in part by the MRSEC Program of the NSF under DMR-0080065. JAH Machining, Dr. John A. Klasik, and Travis Voorhees (Cal Poly Pomona) and Jonathan Harris (Pomona College) are thanked for their technical support. Dr. Perry Cheung is thanked for his active and tireless support in the preparation of this manuscript. Drs. Juan Nava and Jonathan Puthoff are thanked for their careful review of the manuscript. Financial support from Ms. Sylvia Hall, the LA Section of NACE International, Western States Corrosion Seminar, Western Area of NACE International, and the NACE International Foundation is gratefully acknowledged.

REFERENCES

1. M.F. McGuire, *Stainless Steels for Design Engineers* (Materials Park, OH: ASM International, 2008), pp. 69–78.
2. S. Şahim and M. Übeyli, *J. Fus. Energy* 27, 271 (2008).
3. G.W. Goward, *Surf. Coat. Technol.* 108–109, 73 (1998).
4. V.A. Ravi, *ASM Handbook 13A* (Materials Park, OH: ASM International, 2003), pp. 759–771.
5. V.A. Ravi, T.K. Nguyen, and J.C. Nava, *Thermochemical Surface Engineering of Steels*, ed. E.J. Mittemeijer and M.A.J. Somers (Waltham, MA: Elsevier Inc., 2014).
6. V.A. Ravi, J. Koch, C. Kouttjie, and T.K. Nguyen (Paper presented at Stainless Steel World America 2010, Houston, TX, 5–7 October 2010).
7. K. Smith, A. Kutyan, S. Abolian, T. Krenek, S. Salas, and V.A. Ravi, *Corrosion 2013*, Paper No. 2865 (Houston, TX: NACE International, 2013).
8. A. Cuevas, K.J. Schumann, C.J. Simpson, and V.A. Ravi, *Corrosion 2012*, paper no. 1710 (Houston, TX: NACE International, 2012).
9. A. Kvrlyan, C.J. Lopez, S.A. Phipps, B.T. Stoops, Z. Megerdichian, F.H. Ismail, and V.A. Ravi, *Corrosion 2014*, Paper No. 4327 (Houston, TX: NACE International, 2014).
10. Z.D. Xiang and P.K. Datta, *J. Mater. Sci.* 40, 1959 (2005).
11. R. Sakidja, J.H. Perepezko, and P. Calhoun, *Oxid. Metal.* 81, 167 (2014).
12. N.V. Bangaru and R.C. Krutenat, *J. Vac. Sci. Technol. B* 2, 806 (1984).
13. P.S. Korinko and S.H. Malene, *J. Fail. Anal. Prev.* 1, 61 (2001).
14. O. Hammar and U. Svensson, *Solidification and Casting of Metals: Proceedings of an International Conference on Solidification* (London, UK: The Metals Society, 1979), pp. 401–410.
15. H.E. McGannon, *The Making, Shaping and Treating of Steel*, 9th ed. (Pittsburgh, PA: United States Steel Corporation, 1970), p. 1277.
16. H.E. McGannon, *The Making, Shaping and Treating of Steel*, 9th ed. (Pittsburgh, PA: United States Steel Corporation, 1970), p. 1164.